Multiphase Computations in Geometrical Optics

Björn Engquist and Olof Runborg

Abstract. We propose a new set of partial differential equations which can be seen as a generalization of the classical eikonal and transport equations, to allow for solutions with multiple phases. The traditional geometrical optics pair of equations do not include solutions with multiple phases, corresponding to crossing waves. The new partial differential equations form a hyperbolic system of conservation laws with source terms. They are derived from a closure of the kinetic formulation of geometrical optics. Numerical examples are presented.

1. Introduction

In the direct calculation of wave propagation, the computational effort is larger at higher frequencies. With constant accuracy the work grows algebraically with frequency. For sufficiently high frequencies or short wavelengths it is unrealistic to compute the wave field directly. Fortunately, this is often the regime for which high-frequency asymptotic approximations are quite accurate. These geometrical optics type asymptotic expansions are used in many applications, for example in electromagnetic, elastic and acoustic wave propagation.

Traditionally, ray tracing has been the computational method of choice. Recently, however, the geometrical optics approximations are also being solved by partial differential equation (PDE) techniques. This is e.g. done in [5] and within the framework of seismology in [9], [11] and [12]. The traditional PDEs give only one unique phase at each point in space. In this paper we shall derive equations which allow for multiple phases or crossing rays. The equations are based on the closure assumption of a finite number of crossing rays for the kinetic formulation of geometrical optics.

1.1. High-Frequency Asymptotics

When high-frequency waves are treated, the computations can be simplified by considering the asymptotic behavior of the solution as the frequency tends to infinity. There are two strongly related ways to formulate this approximation: the PDEs of geometrical optics and ray tracing. Typical wave phenomena, such as diffraction and interference, are lost in the leading terms of the high-frequency approximation.

Classical geometrical optics is based on the scalar wave equation,

$$u_{tt} + c^2\boldsymbol{\nabla}^2 u = 0. \tag{1}$$

Here $c = c(\boldsymbol{x})$ is the local wave velocity of the medium. We also define the *index of refraction* as $\eta = c_0/c$ with the reference velocity c_0 (e.g. the speed of light in vacuum). Geometrical optics considers the case when the solution to (1) can be written as a series expansion of the form:

$$u = e^{i\omega\phi(\boldsymbol{x},t)} \sum_{k=0}^{\infty} w_k(\boldsymbol{x},t)(i\omega)^{-k}. \tag{2}$$

Entering this expression into (1), we obtain separate equations for the unknown variables in (2). The phase function ϕ will satisfy the *eikonal equation*,

$$\phi_t + c|\boldsymbol{\nabla}\phi| = 0, \tag{3}$$

and the first amplitude coefficient w_0 solves the *transport equation*,

$$(w_0)_t + c\frac{\boldsymbol{\nabla}\phi\cdot\boldsymbol{\nabla}w_0}{|\boldsymbol{\nabla}\phi|} + \frac{c^2\boldsymbol{\nabla}^2\phi - \phi_{tt}}{2c|\boldsymbol{\nabla}\phi|}w_0 = 0. \tag{4}$$

Note that once ϕ is known, the transport equation is a linear equation with variable coefficients.

The problem with the geometrical optics approach is that the class of solutions which justify an expansion of the type (2) is limited. In particular, it does not include solutions with multiple phases, corresponding to crossing waves. In fact, even in the case of a single phase solution, the series does not necessarily converge, for instance when the geometric boundaries create diffraction effects. We shall concentrate on the multiple phase problem.

The eikonal equation is a nonlinear PDE which requires extra conditions to have a unique solution. This solution is known as the *viscosity solution* [3]. At points where the correct solution should have a multi-valued phase, the viscosity solution picks out the phase corresponding to the first arriving wave. In the case of the linear wave equation, clearly, a linear combination of solutions is also a solution. For the nonlinear eikonal equation, this superposition principle does not hold.

Solving the eikonal equation numerically as a PDE instead of using ray tracing has recently been used in seismology. This technique is demonstrated in [9], [11] and [12]. For these applications it is of direct interest to determine the first arrival. A second phase, corresponding to crossing rays was calculated in [5] using two separate eikonal equations. Boundary conditions for the second phase was given at the discontinuity of the first phase or at a geometric reflecting boundary. This boundary could be difficult to determine.

Another way to treat high-frequency waves computationally is through ray tracing, which is based on a kinetic formulation. The waves are postulated to be particles (photons) whose trajectories are rays. The *ray vector*, $\boldsymbol{p}$, is defined as the index of refraction multiplied by the unit vector, $\hat{\boldsymbol{s}}$, in the direction of the ray, i.e. $\boldsymbol{p} = \eta\hat{\boldsymbol{s}}$. For simplicity we will henceforth let $c_0 = 1$, so that the velocity vector $\boldsymbol{v} = c\hat{\boldsymbol{s}} = c^2\boldsymbol{p}$. A transport equation for particles in the space $(\boldsymbol{x}, \boldsymbol{p}, t)$ can then be derived. Denoting the density of particles by $f(\boldsymbol{x}, \boldsymbol{p}, t)$ the evolution of f is described by the Vlasov type equation

$$f_t + \boldsymbol{v} \cdot \boldsymbol{\nabla}_x f + c\boldsymbol{\nabla}_x \eta \cdot \boldsymbol{\nabla}_p f = 0. \tag{5}$$

This follows from the Hamiltonian system with

$$H = \frac{1}{2}\left[\frac{|\boldsymbol{p}|^2}{\eta^2} - 1\right]. \tag{6}$$

Tracing the particle trajectories of (5) corresponds to ray tracing and also to the method of characteristics for (3) and (5). Since (5) is linear the superposition principle is valid.

Because of the large number of independent variables (six in 3D) it is very hard to solve the full equation (5) numerically. If the equation is solved using ray tracing it is difficult to cover the full domain with rays, [11].

1.2. Moment Formulation

In this paper we propose a middle way between geometrical optics and the kinetic model. The technique we use to capture multi-valued solutions is based on a closure assumption for a system of equations representing the moments (see [1]). The starting point for this approach is the transport equation (5). Instead of solving the full equation in phase space, we observe that when f is of a simple form in $\boldsymbol{p}$, we can transform (5) to a finite system of moment equations in the reduced space $(\boldsymbol{x}, t)$, analogously to the classical approach of the hydrodynamic limit from a kinetic formulation. We are interested in cases corresponding to a finite number of rays in different directions at each point.

This paper is organized as follows: In Section 2 the moment equations are derived from the kinetic model for high-frequency waves. The system is essentially closed and equivalent to the equations of geometrical optics. We also explore some theoretical issues and find that the resulting hyperbolic equations are not well-posed in the strong sense. Furthermore, we present the solution of the Riemann problem and show that there is no entropy for the one-dimensional system. Finally, in Section 3, we discuss numerical approximations for the equations as well as results of numerical experiments.

2. Moment Equations

In this section we will derive and analyze the system of PDEs that follows from the kinetic model and the assumption that a maximum of N rays pass through any given point in space. The analysis is carried out in two-dimensional space.

2.1. Derivation of the Moment Equations

We start by defining the moments m_{ij}. With $\boldsymbol{p} = (p_1, p_2)$, let

$$m_{ij} = \int_{\mathbb{R}^2} p_1^i p_2^j f d\boldsymbol{p}. \tag{7}$$

Next, we multiply (5) by $p_1^i p_2^j$ and integrate over $\mathbb{R}^2$ with respect to $\boldsymbol{p}$. Using the definition (7) we get the moment equation,

$$(\eta^2 m_{ij})_t + (m_{i+1,j})_x + (m_{i,j+1})_y = i\eta\eta_x m_{i-1,j} + j\eta\eta_y m_{i,j-1}, \tag{8}$$

where we have used the fact that f has compact support in $\boldsymbol{p}$. Since this equation is valid for all $i, j \geq 0$, we have an infinite system of moment equations. For uniformity in notation we have defined $m_{i,-1} = m_{-1,i} = 0$, $\forall i$.

The system (8) is not closed. If truncated at finite i and j, there are more unknowns than equations. To close (8) we use the assumption that for fixed values of $\boldsymbol{x}$ and t, the particle density f can be written

$$f(\boldsymbol{x}, \boldsymbol{p}, t) = \sum_{k=1}^{N} g_k \cdot \delta(|\boldsymbol{p}| - \eta, \arg \boldsymbol{p} - \theta_k). \tag{9}$$

The new variables that we have introduced here are $g_k = g_k(\boldsymbol{x}, t)$, which corresponds to the strength (particle density) of ray k, and $\theta_k = \theta_k(\boldsymbol{x}, t)$ which is the direction of the same ray. Inserting (9) into (7) yields

$$m_{ij} = \sum_{k=1}^{N} \eta^{i+j} g_k \cos^i \theta_k \sin^j \theta_k. \tag{10}$$

A system describing N phases, needs $2N$ equations, corresponding to the N ray strengths g_k and their directions θ_k. We choose here the equations for the moments $m_{2k-1,0}$ and $m_{0,2k-1}$ with $k = 1, \ldots, N$. This system can be essentially closed for all N (see Section 2.3). After scaling the moments, $m_{ij} := \eta^{-i-j} m_{ij}$, and introducing the new variables

$$\boldsymbol{u} = (u_1, \ldots, u_{2N})^T := (g_1 \cos\theta_1, g_1 \sin\theta_1, \ldots, g_N \cos\theta_N, g_N \sin\theta_N)^T. \tag{11}$$

we get a system of nonlinear conservation laws with source terms,

$$\boldsymbol{F}_0(\eta^2 \boldsymbol{u})_t + \boldsymbol{F}_1(\eta \boldsymbol{u})_x + \boldsymbol{F}_2(\eta \boldsymbol{u})_y = \boldsymbol{K}(\boldsymbol{u}, \eta_x, \eta_y), \tag{12}$$

where the functions $\boldsymbol{F}_k$ and $\boldsymbol{K}$ are rather complicated nonlinear functions, which depend on the particular choice of moments above. A different choice of moments gives different functions. Equivalently, with

$$\hat{\boldsymbol{m}} = (m_{10}, m_{01}, m_{30}, m_{03}, \ldots, m_{2N-1,0}, m_{0,2N-1})^T, \tag{13}$$

we could write (12) as

$$(\eta^2 \hat{\boldsymbol{m}})_t + \boldsymbol{F}_1 \circ \boldsymbol{F}_0^{-1}(\eta \hat{\boldsymbol{m}})_x + \boldsymbol{F}_2 \circ \boldsymbol{F}_0^{-1}(\eta \hat{\boldsymbol{m}})_y = \boldsymbol{K}(\boldsymbol{F}_0^{-1}(\hat{\boldsymbol{m}}), \eta_x, \eta_y). \tag{14}$$

In the most simple case, $N = 1$, the function $\boldsymbol{F}_0$ is the identity and

$$\boldsymbol{F}_1 = \frac{u_1}{|\boldsymbol{u}|}\begin{pmatrix} u_1 \\ u_2 \end{pmatrix}, \quad \boldsymbol{F}_2 = \frac{u_2}{|\boldsymbol{u}|}\begin{pmatrix} u_1 \\ u_2 \end{pmatrix}, \quad \boldsymbol{K} = \frac{\eta_x u_2 - \eta_y u_1}{|\boldsymbol{u}|}\begin{pmatrix} u_2 \\ -u_1 \end{pmatrix}. \tag{15}$$

For $N = 2$, let $\boldsymbol{w} = (w_1, w_2)^T$ and

$$\boldsymbol{f}_0 = \begin{pmatrix} w_1 \\ w_2 \\ w_1^3/|\boldsymbol{w}|^2 \\ w_2^3/|\boldsymbol{w}|^2 \end{pmatrix}, \qquad \boldsymbol{f}_1 = \frac{w_1}{|\boldsymbol{w}|}\boldsymbol{f}_0, \qquad \boldsymbol{f}_2 = \frac{w_2}{|\boldsymbol{w}|}\boldsymbol{f}_0,$$

$$\boldsymbol{k} = \frac{\eta_x w_2 - \eta_y w_1}{|\boldsymbol{w}|}\begin{pmatrix} w_2 \\ -w_1 \\ w_1^2 w_2/|\boldsymbol{w}|^2 \\ -w_1 w_2^2/|\boldsymbol{w}|^2 \end{pmatrix}. \tag{16}$$

Then $\boldsymbol{F}_k = \boldsymbol{f}_k(u_1, u_2) + \boldsymbol{f}_k(u_3, u_4)$ for $k = 0, 1, 2$ and $\boldsymbol{K} = \boldsymbol{k}(u_1, u_2) + \boldsymbol{k}(u_3, u_4)$.

2.2. A Comparison with Geometrical Optics

For smooth solutions, the moment equations (12) are an equivalent formulation of the equations of geometrical optics. Suppose $\{w_{0,k}\}_{k=1}^N$ and $\{\phi_k\}_{k=1}^N$ are the solutions of N pairs of eikonal- and transport equations, (3, 4). Then, if

$$g_k = w_{0,k}^2, \qquad \cos\theta_k = \frac{(\phi_k)_x}{|\boldsymbol{\nabla}\phi_k|}, \qquad \sin\theta_k = \frac{(\phi_k)_y}{|\boldsymbol{\nabla}\phi_k|}, \qquad k = 1, \ldots, N, \tag{17}$$

the corresponding $\boldsymbol{u}$, defined in (11), will solve (12), see [10]. As expected the vector $(u_{2k-1}, u_{2k})^T$ points in the direction of the gradient of ϕ_k. The length of the vector corresponds to the first amplitude coefficient squared.

2.3. Closure of the Moment Equations

The system (12) is closed if and only if the flux functions $\boldsymbol{F}_1 \circ \boldsymbol{F}_0^{-1}(\hat{\boldsymbol{m}})$ and $\boldsymbol{F}_2 \circ \boldsymbol{F}_0^{-1}(\hat{\boldsymbol{m}})$ are well defined for all solutions, $\hat{\boldsymbol{m}}$, to (14) at all times. This can be proved as long as no two rays meet head-on. To be more precise, introduce the complex variables

$$z_k(\boldsymbol{x}, t) = \cos\theta_k(\boldsymbol{x}, t) + i\sin\theta_k(\boldsymbol{x}, t), \qquad k = 1, \ldots, N, \tag{18}$$

so that $g_k z_k = u_{2k-1} + i u_{2k}$. Then the following theorem holds.

Theorem 2.1. *Let $\boldsymbol{F}_k$ be the functions in (12), corresponding to the moment vector $\hat{\boldsymbol{m}}$ defined in (13). Let $\boldsymbol{F}_0|\mathcal{D}$ be the restriction of $\boldsymbol{F}_0$ to the domain*

$$\mathcal{D} = \{\boldsymbol{u} \in \mathbb{R}^{2N} \mid z_k + z_\ell \neq 0, \ \forall k, \ell\}, \tag{19}$$

with z_k defined as in (18). For $\hat{\boldsymbol{m}} \in \boldsymbol{F}_0(\mathcal{D})$ the flux functions

$$\boldsymbol{F}_1 \circ (\boldsymbol{F}_0|\mathcal{D})^{-1}(\hat{\boldsymbol{m}}), \qquad \boldsymbol{F}_2 \circ (\boldsymbol{F}_0|\mathcal{D})^{-1}(\hat{\boldsymbol{m}}) \tag{20}$$

are well defined.

The proof can be found in [10]. Note, with a different choice of $\hat{\boldsymbol{m}}$, Theorem 2.1 does not necessarily hold, see [10].

2.4. Analysis of the Conservation Laws

For simplicity we will mainly deal with the single phase, $N = 1$, one-dimensional case where the medium is vacuum, $\eta = \text{const} = 1$. With the $\boldsymbol{u}$ variables defined in (11) as conserved quantities, the system can be written on the standard form of a conservation law,

$$\boldsymbol{u}_t + \boldsymbol{f}(\boldsymbol{u})_x = 0, \qquad \boldsymbol{f}(\boldsymbol{u}) = \frac{u_1}{|\boldsymbol{u}|}\begin{pmatrix} u_1 \\ u_2 \end{pmatrix}. \tag{21}$$

The Jacobian of $\boldsymbol{f}$ with respect to $\boldsymbol{u}$ has the following form:

$$\frac{\partial \boldsymbol{f}}{\partial \boldsymbol{u}} = G\begin{pmatrix} \cos\theta & -\sin\theta \\ 0 & \cos\theta \end{pmatrix}G^{-1}, \qquad G = \begin{pmatrix} \cos\theta & -\sin\theta \\ \sin\theta & \cos\theta \end{pmatrix}. \tag{22}$$

Thus, the linearized problem has a double real eigenvalue, $\cos\theta$, and an incomplete set of eigenvectors; the system (21) is only *weakly hyperbolic*. In general this means that (21) is not well-posed in the strongly hyperbolic sense. The solution of the linearized problem with frozen coefficients loses one derivative. The L_2 norm of the solution at time $t > t_0$ can be estimated in terms of the H_1 norm of the initial data at time $t = t_0$. There is no bounded variation estimate for (21) and one can expect delta function type measure solutions. Such solutions appear when the correct physical solution contains more phases than the system can describe, cf. Figure 6. See [2] and [4] for analysis of related problems.

It is interesting again to compare the moment equations with the eikonal and transport equations, (3) and (4). The latter also form a weakly hyperbolic system with the same eigenvalue as (21). The viscosity solution may have a jump in $\boldsymbol{\nabla}\phi$. Because of the term $\boldsymbol{\nabla}^2\phi$ in the source term of (4), the first amplitude coefficient w_0 has a measure at these points.

In the general case with N phases, homogeneous medium, the governing equations read

$$\boldsymbol{F}_0(\boldsymbol{u})_t + \boldsymbol{F}_1(\boldsymbol{u})_x = 0. \tag{23}$$

Denoting the Jacobians of $\boldsymbol{F}_k$ with J_k, the following relationship can be derived:

$$J_1 = J_0 \cdot \operatorname{diag}\left(\frac{\partial \boldsymbol{f}}{\partial \boldsymbol{u}}(\theta_1), \ldots, \frac{\partial \boldsymbol{f}}{\partial \boldsymbol{u}}(\theta_N)\right). \tag{24}$$

This shows that the eigenvalues of the general system are simply the union of the eigenvalues of N systems of the type (21). It also shows that there will not be more than N eigenvectors, for the $2N \times 2N$ system. Hence, we have shown that the system (23) is weakly hyperbolic. This also holds for the full 2D system (12), see [10].

2.5. The Riemann Problem

We study the one-dimensional Riemann problem for (21),

$$\boldsymbol{u}_t + \boldsymbol{f}(\boldsymbol{u})_x = 0, \qquad \boldsymbol{u}(x,0) = \begin{cases} \boldsymbol{u}_l & x < 0, \\ \boldsymbol{u}_r & x > 0. \end{cases} \tag{25}$$

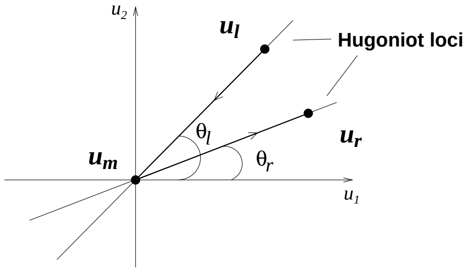

FIGURE 1. Hugoniot loci for left and right state, and solution to the Riemann problem for the first type of discontinuity, plotted in phase space.

At a discontinuity the conservation form gives the Rankine-Hugoniot jump condition,

$$\boldsymbol{f}(\boldsymbol{u}_l) - \boldsymbol{f}(\boldsymbol{u}_r) = s(\boldsymbol{u}_l - \boldsymbol{u}_r), \tag{26}$$

where s represents the propagation speed of the discontinuity. Since $\boldsymbol{f}(\boldsymbol{u}) = \cos\theta \boldsymbol{u}$, this simplifies to

$$\cos\theta_l \boldsymbol{u}_l - \cos\theta_r \boldsymbol{u}_r = s(\boldsymbol{u}_l - \boldsymbol{u}_r). \tag{27}$$

In our case the Hugoniot locus of state $\boldsymbol{u}_l$ is simply $\alpha\boldsymbol{u}_l$, $\alpha \in \mathbb{R}$. The speed of propagation is $s = \cos\theta_l$. There will be two types of discontinuities. If $\cos\theta_l < \cos\theta_r$, we can use the origin of the phase space as the intermediate state, hence $\boldsymbol{u}_m = 0$. The Hugoniot loci and the solution for this type of discontinuity is illustrated in Figure 1. If $\cos\theta_l > \cos\theta_r$, on the other hand, we do not have a solution in a classical sense. Formally, however, a weak solution to the conservation law with this initial data is given by setting $\boldsymbol{u}_m = t\tilde{\boldsymbol{u}}_m\delta(x - st)$. The conservation form gives a slightly modified jump condition for this case,

$$\cos\theta_l \boldsymbol{u}_l - \cos\theta_r \boldsymbol{u}_r = \cos\tilde{\theta}_m(\boldsymbol{u}_l - \boldsymbol{u}_r) + \tilde{\boldsymbol{u}}_m, \tag{28}$$

with the propagation speed $s = \cos\tilde{\theta}_m$.

It is easily verified from (22). that $\boldsymbol{u}$ itself is an eigenvector of the Jacobian of $\boldsymbol{f}$. Therefore, the Hugoniot locus will coincide with the integral curves of the system's characteristic fields. Since the (double) eigenvalue of (22), $\cos\theta$, is constant along the curves, the fields are linearly degenerate. From this we conclude that the first type of discontinuity is a linear, contact discontinuity; characteristics run parallel to the discontinuity. The linear degeneracy also excludes the possibility of rarefaction wave solutions.

The second type of discontinuity will always have two characteristics incident to the discontinuity at each side, because of the double eigenvalue. These discontinuities are thus of overcompressive shock type. The two different discontinuities, plotted in (x, t)-space, are shown in Figure 2.

For the analysis of (21) it would be useful to find an entropy function corresponding to the system. This is, however, not possible.

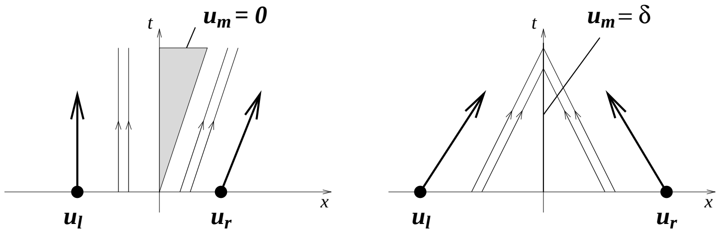

FIGURE 2. The two different types of discontinuities: contact discontinuity (left) and overcompressive shock (right).

Theorem 2.2. *There exists no twice continuously differentiable convex entropy pair for the system (21).*

Proof. Let $\boldsymbol{u}$ be a smooth solution to (21) and $U, F \in C^2$ satisfy

$$U(\boldsymbol{u})_t + F(\boldsymbol{u})_x = 0. \tag{29}$$

Then multiplication of (21) by $\boldsymbol{\nabla} U$ and identification gives that $\boldsymbol{\nabla} U \frac{\partial \boldsymbol{f}}{\partial \boldsymbol{u}} = \boldsymbol{\nabla} F$. Now, it turns out that

$$\frac{u_1(u_1^2 U_{u_1,u_1} + 2u_1u_2U_{u_1,u_2}u_2^2U_{u_2,u_2})}{(u_1^2+u_2^2)^{3/2}} = \boldsymbol{\nabla} \times (\boldsymbol{\nabla} U \frac{\partial \boldsymbol{f}}{\partial \boldsymbol{u}}) = \boldsymbol{\nabla} \times \boldsymbol{\nabla} F = 0. \tag{30}$$

Therefore, with $H(U)$ denoting the Hessian of U,

$$\det H(U) = U_{u_1,u_1}U_{u_2,u_2} - U_{u_1,u_2}^2 = -\frac{1}{4}\Big(\frac{u_1}{u_2}U_{u_1,u_1} - \frac{u_2}{u_1}U_{u_2,u_2}\Big)^2 \leq 0. \tag{31}$$

3. Numerical Treatment

This section includes some results on the numerical treatment of (12). As was discussed in the previous section, the system (12) is only weakly hyperbolic. This makes it sensitive and creates problems for the numerical methods.

The point of departure for our numerical approximations is the basic first order accurate *Lax-Friedrichs* finite difference method. Less smearing of shocks is obtained with the *Godunov* method (see e.g. [7]). For (12) it may, however, produce large L_∞ errors even for smooth problems, cf. Figure 3. The reason for the method's behavior in Figure 3 can be found in the analysis of the Riemann problem in Section 2.5. Along the line $y = 1$ the Riemann problem in the y-direction corresponds to the situation in Figure 2 (left). Since there is no rarefaction wave solution, there will be no flux in the y direction, and the method reduces to the one-dimensional Godunov method in the x-direction along this line. Hence, along $y = 1$ there will be pure transport, and no damping.

We have also implemented the *Nessyahu-Tadmor* method, [8]. It is a second order TVD method based on the Lax-Friedrichs structure. The results have been very satisfactory when the algorithm was implemented without dimensional

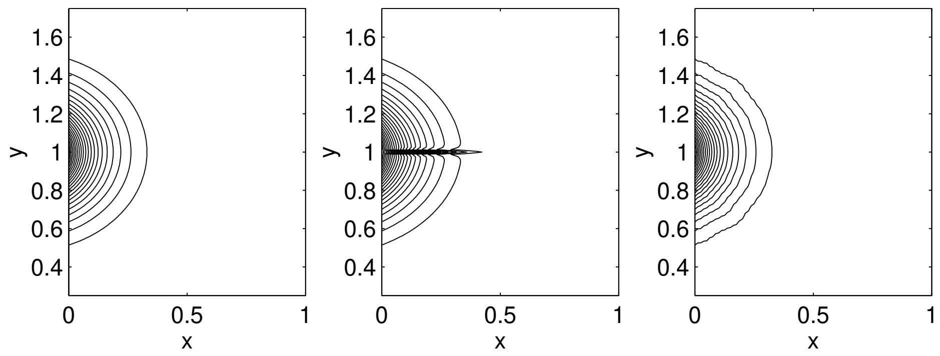

FIGURE 3. Test case with a smooth point source located at $(-0.2, 1)$. Figure shows contour plot of the ray strength $g = m_{00}$ of the single phase system, solved using Lax-Friedrichs (left), Godunov (middle) and splitted Nessyahu-Tadmor (right). Note the problems with using the last two methods.

splitting. With splitting, the convergence rate is poorer, in particular in L_∞, cf. Figure 3. See [6] for a further discussion.

In the multiple phase case, we have mainly considered the case of two and three phases, and we have only used the Lax-Friedrichs method, see Figures 4–6. A more complete descriptions of the results for the test cases presented here, and others, can be found in [10].

It is more difficult to get reliable calculations when solving (12) with multiple phases, than in the case of a single phase. At each grid point it is necessary to solve a nonlinear system of equations of the type $\boldsymbol{F}_0(\boldsymbol{u}) = \hat{\boldsymbol{m}}$ and in some cases this system had to be solved in the least squares sense.

References

[1] Y. Brenier and L. Corrias. Capturing multivalued solutions. CAM Report 94-46, Department of Mathematics, UCLA, 1994.

[2] Y. Brenier and E. Grenier. On the model of pressureless gases with sticky particles. CAM Report 94-45, Department of Mathematics, UCLA, 1994.

[3] M. Crandall and P. Lions. Viscosity solutions of Hamilton-Jacobi equations. *Transactions of the American Mathematical Society*, 277:1–42, 1983.

[4] W. E, Yu. G. Rykov, and Ya. G. Sinai. Generalized variational principles, global weak solutions and behavior with random initial data for systems of conservation laws arising in adhesion particle dynamics, to appear.

[5] B. Engquist, E. Fatemi, and S. Osher. Numerical solution of the high frequency asymptotic expansion for the scalar wave equation. CAM Report 93-05, Department of Mathematics, UCLA, 1993.

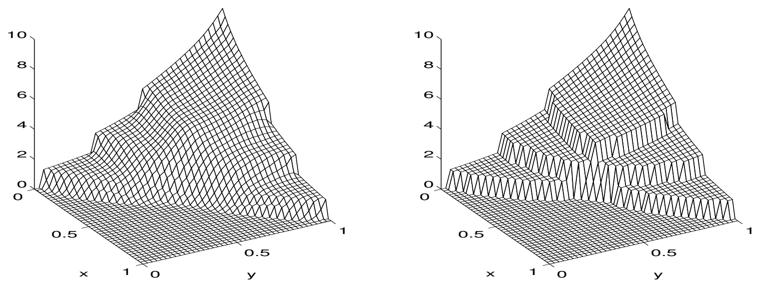

Figure 4. Test case with three discontinuous point sources, located at coordinates $(-0.4, 0.8)$, $(0.2, 1.4)$ and $(-0.15, 1.15)$. Figure shows combined strengths of the three waves of the three phase system, $g_1+g_2+g_3 = m_{00}$, computed with Lax-Friedrichs method (left) and exact (right).

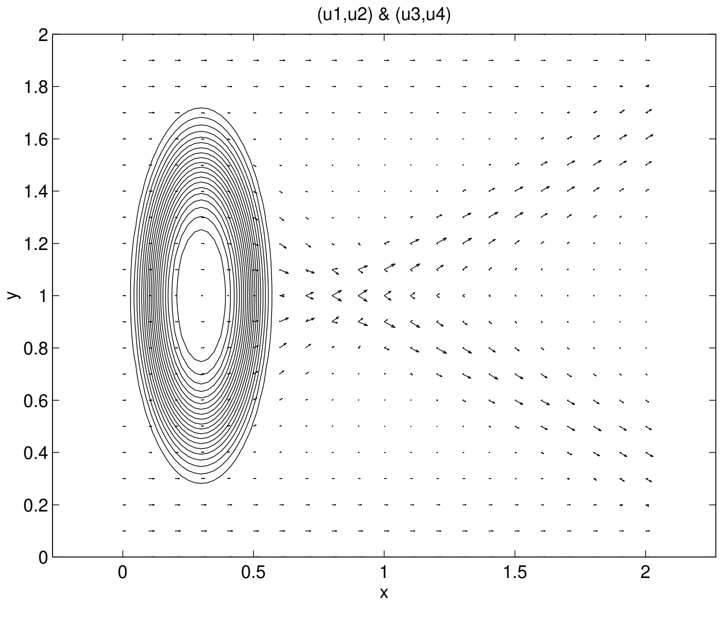

Figure 5. Test case with inhomogeneous medium, modeling a smooth convex lens. A plane wave enters from the left. Figure shows vector fields (u_1, u_2), (u_3, u_4) of the two phase system, solved using Lax-Friedrichs, and contour lines of the index of refraction η superimposed.

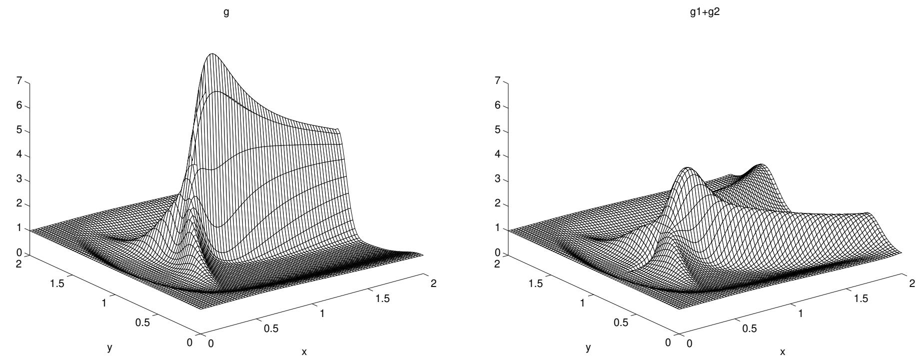

FIGURE 6. Same test case as in Figure 5. Figure shows ray strength g for one phase system (left) and combined ray strengths $g_1 + g_2 = m_{00}$ for two phase system (right). Note how one phase is not sufficient to describe the physically correct solution, so a measure solution is indicated to the left.

[6] G.-S. Jiang and E. Tadmor. Non-oscillatory central schemes for multidimensional hyperbolic conservation laws. CAM Report 96-36, Department of Mathematics, UCLA, 1996.

[7] R. J. LeVeque. *Numerical Methods for Conservation Laws.* Birkhäuser, 1992.

[8] H. Nessyahu and E. Tadmor. Non-oscillatory central differencing for hyperbolic conservation laws. *Journal of Computational Physics*, 87(2):408–463, 1990.

[9] F. Qin et al. Finite-difference solution of the eikonal equation along expanding wavefronts. *Geophysics*, 57(3):478–487, March 1992.

[10] O. Runborg. Multiphase computations in geometrical optics. Licentiate's Thesis TRITA-NA-9609, Department of Numerical Analysis and Computing Science, KTH, 1996.

[11] J. van Trier and W. W. Symes. Upwind finite-difference calculation of traveltimes. *Geophysics*, 56(6):812–821, June 1991.

[12] J. Vidale. Finite-difference calculation of traveltimes. *Bulletin of the Seismological Society of America*, 78(6):2062–2076, December 1988.

Department of Numerical Analysis and Computing Science
Royal Institute of Technology
S-100 44 Stockholm, Sweden
E-mail address: `engquist@math.ucla.edu, olofr@nada.kth.se`